Microvascular Research 92 (2014) 62–71

Contents lists available at ScienceDirect

Microvascular Research

journal homepage: www.elsevier.com/locate/ymvre

Functional slit lamp biomicroscopy for imaging bulbar conjunctival microvasculature in contact lens wearers

Hong Jiang [a,b,*,1], Jianguang Zhong [a,c,1], Delia Cabrera DeBuc [a], Aizhu Tao [a,d], Zhe Xu [a,d], Byron L. Lam [a], Che Liu [a,e], Jianhua Wang [a]

[a] Bascom Palmer Eye Institute, University of Miami, Miami, FL, USA
[b] Department of Neurology, University of Miami, Miami, FL, USA
[c] Department of Ophthalmology, Hangzhou First People's Hospital, Hangzhou, Zhejiang, China
[d] School of Ophthalmology and Optometry, Wenzhou Medical College, Wenzhou, Zhejiang, China
[e] Department of Biomedical Engineering, University of Miami, Miami, FL, USA

ARTICLE INFO

Article history:
Accepted 7 January 2014
Available online 17 January 2014

ABSTRACT

Purpose: To develop, test and validate functional slit lamp biomicroscopy (FSLB) for generating non-invasive bulbar conjunctival microvascular perfusion maps (nMPMs) and assessing morphometry and hemodynamics.
Methods: FSLB was adapted from a traditional slit-lamp microscope by attaching a digital camera to image the bulbar conjunctiva to create nMPMs and measure venular blood flow hemodynamics. High definition images with a large field of view were obtained on the temporal bulbar conjunctiva for creating nMPMs. A high imaging rate of 60 frames per second and an ~210× high magnification were achieved using the camera inherited high speed setting and Movie Crop Function, for imaging hemodynamics. Custom software was developed to segment bulbar conjunctival nMPMs for further fractal analysis and quantitatively measure blood vessel diameter, blood flow velocity and flow rate. Six human subjects were imaged before and after 6 h of wearing contact lenses. Monofractal and multifractal analyses were performed to quantify fractality of the nMPMs.
Results: The mean bulbar conjunctival vessel diameter was 18.8 ± 2.7 μm at baseline and increased to 19.6 ± 2.4 μm after 6 h of lens wear ($P = 0.020$). The blood flow velocity was increased from 0.60 ± 0.12 mm/s to 0.88 ± 0.21 mm/s ($P = 0.001$). The blood flow rate was also increased from 129.8 ± 59.9 pl/s to 207.2 ± 81.3 pl/s ($P = 0.001$). Bulbar conjunctival nMPMs showed the intricate details of the bulbar conjunctival microvascular network. At baseline, fractal dimension was 1.63 ± 0.05 and 1.71 ± 0.03 analyzed by monofractal and multifractal analyses, respectively. Significant increases in fractal dimensions were found after 6 h of lens wear ($P < 0.05$).
Conclusions: Microvascular network's fractality, morphometry and hemodynamics of the human bulbar conjunctiva can be measured easily and reliably using FSLB. The alternations of the fractal dimensions, morphometry and hemodynamics during contact lens wear may indicate ocular microvascular responses to contact lens wear.

Introduction

The characterization and quantification of morphometric and dynamic microvascular abnormalities play a crucial role in the understanding of pathophysiology and optimization of treatments for microangiopathy. The microvasculature of the bulbar conjunctiva can be easily accessed and is suitable for in vivo real-time imaging under physiological and pathological conditions including ocular, systemic and central nervous system diseases. The blood flow velocity of the bulbar conjunctival microvasculature has been studied mainly by using videography in patients with diabetes (Cheung et al., 2009a, 2001b), contact lens wearers (Cheung et al., 2012) and cerebral small vessel disease in rates (Schreiber et al., 2013). Using computer-assisted intravital microscopy (CAIM), Cheung and associates reported bulbar conjunctival vessels with significantly enlarged diameters and uneven distributions in the bulbar conjunctiva of type 2 diabetic patients (Cheung et al., 2001b). The researchers found that morphometric changes in diabetic microvasculature presented earlier in the bulbar conjunctiva than in the retina (To et al., 2011).

The eye and the brain share the same blood supply, which originates from the internal carotid artery (ICA), and have similar branching patterns. Blood flow through the bulbar conjunctiva, the terminal vascular bed of the ICA, has been used to monitor cerebral blood flow during aortic arch surgery (Ohtani, 1996) and in a previous study was found to be attenuated when the ICA was clamped (Schaser et al., 2003). Low bulbar conjunctival blood flow velocity measured by CAIM correlates with high

* Corresponding author at: Bascom Palmer Eye Institute, University of Miami, Miller School of Medicine, 1638 NW 10th Avenue, Clinical Research Building — Room 1557, Miami, FL 33136, USA.
E-mail address: hjiang@med.miami.edu (H. Jiang).
[1] Contributed equally to the work.

0026-2862/$ – see front matter © 2014 Elsevier Inc. All rights reserved.
http://dx.doi.org/10.1016/j.mvr.2014.01.005

blood flow velocities measured by Trans-Cranial Doppler (TCD) and is regarded as an indicator of increased risk of stroke in sickle cell patients (Cheung et al., 2001a). Studying the bulbar conjunctival microvascular network, morphometry, and hemodynamics may reveal early signs of disease, which may ultimately lead to the development of image biomarkers using the bulbar conjunctiva microvasculature.

A fractal is a mathematical set with a fractal dimension that differs from its topological dimension (Talu, 2011). Fractal analysis is used to assess fractal characteristics, and fractal dimensions are capable of revealing the differences and irregularities in these structures (Liew et al., 2008). Fractal analysis has been extensively used to investigate the changes in the retinal vascular complexity and branching density (Avakian et al., 2002; Azemin et al., 2011; Cheung et al., 2010; Liew et al., 2008; Macgillivray and Patton, 2006). It has been used to analyze retinal vascular trees in fundus photographs and fluorescein angiography images to quantitatively measure the microvascular damage in diabetes (Avakian et al., 2002; Cheung et al., 2009b; Lim et al., 2009) and lacunar infarcts (Cheung et al., 2010; Doubal et al., 2010).

To the best of our knowledge, simultaneous measurement of the blood flow velocity in bulbar conjunctival vessels and their network complexity has not been fully explored due to technical difficulties. We developed an imaging modality, functional slit lamp biomicroscopy (FSLB), which uses a simple adaptation of traditional slit-lamp microscope to image both the bulbar conjunctival microvascular network and hemodynamics. The goal was to demonstrate and validate FSLB for imaging bulbar conjunctival microvasculature in contact lens wearers.

Materials and methods

Functional slit-lamp microscopy

A digital camera (Canon 60D, Canon Inc., Melville, NY) was attached to a traditional slit-lamp (Nikon FS-2, Nikon Inc., Melville, NY). According to the camera manufacturer, the Canon EOS 60D camera is a complementary metal-oxide semiconductor (CMOS) based digital single lens reflex (DSLR) camera with an imaging sensor size of 22.3 mm × 14.9 mm to acquire a maximum resolution of 5184 × 3456 pixels (~17.9 megapixels). The pixel dimension on the camera sensor is 4.3 μm × 4.3 μm. The International Standards Organization (ISO) sensitivity is up to 6400 expandable to 12,800. The maximum resolution at 60 frames per second (fps) is 640 × 480 pixels for video recording with a telephoto effect, called Movie Crop Function.

The camera has a Movie Crop Function, enabling an equivalent ~7.5× magnification without the loss of image quality for high speed video recording at 60 fps. The Movie Crop Function crops the image directly from the camera sensor at the full standard-definition resolution to preserve image quality and increases telephoto effect, increasing magnification up to 7.5×. In this case, the image resolution of the video sequence is 640 × 480 pixels which are cropped from the center portion of the camera sensor and the pixel interval remains the same as the maximum image resolution of the entire sensor. This function is not the digital zooming found in many compact digital cameras, which only increase the sizes of the pixels, e.g. increasing pixel intervals. To illustrate the Movie Crop Function, the image (Fig. 1A) of the US Air Force 1951 resolution test card with the maximum resolution was captured through FSLB with the optical magnification of 30×. The image (Fig. 1A) had a resolution of 5184 × 3456 pixels (17.9 megapixels) with the field of view of 7.61 × 5.04 mm^2 (1.47 μm per pixel). In the cropped image (Fig. 1B) which simulated the Movie Crop Function for the telephoto effect of 7.5× high magnification, only the center portion of 640 × 480 pixels was cropped with a field of view of 0.94 × 0.70 mm^2 (1.47 μm per pixel). The black and white bars were readable at the element 3 of the group 7 on the resolution card. To compare with the digital zooming, the same image (Fig. 1A) was resized to 720 × 480 pixels, which was about the standard definition video resolution. The image was then digitally resized back to 5184 × 3456 pixels (Fig. 1C). The center 640 × 480 pixels of the resized image were cropped (Fig. 1D). The bars are readable at the element 4 of the group 5. Apparently, the resolution of Fig. 1D was much worse than the simulated image (Fig. 1B) with the Movie Crop Function.

The camera was attached to the slit-lamp via an inherent camera port (Figs. 2A and B). With the inherent optical magnifications of up to 30× in the slit-lamp, the total magnification with the Movie Crop Function can be set up to ~210×. The tested spatial display resolution using a resolution test card (US Air Force 1951, Edmund Optics Inc., Barrington, NJ) was 161 line pairs/mm (Fig. 2C), representing an extremely high resolution (Ye et al., 2013). The width of 1 black or while line of the element 3 in group 7 is 3.11 μm. The setup is sufficient to image the red blood cell (RBC) aggregate movement for the measurement of blood flow velocity, flow rate and vessel diameter (Fig. 2D). A high definition monitor (Samsung, model UN22D5003BF, Samsung Electronics America Inc., Ridgefield Park, NJ) was connected with the camera via a high-definition multimedia interface (HDMI) cable.

The selection of the slit-lamp and special camera function makes the instrumentation simple and easy. The only modification was the use of a Nikon to Canon adapter (Fotodiox, Waukegan, IL) (Fig. 2A). This approach avoided complicated optics for high magnification (Cheung et al., 1999; Koutsiaris et al., 2007; Shahidi et al., 2010) and the use of the state-of-the-art image acquisition hardware (e.g. high speed camera and video acquisition card) (Koutsiaris et al., 2010; Shahidi et al., 2010).

Imaging bulbar conjunctival hemodynamics

A typical magnification for reliable measurement of RBC velocity requires to provide at least one pixel and at best a few pixels for one RBC (~7 μm) to obtain a good signal-to-noise ratio (Deneux et al., 2012). Our system had 1.46 μm per pixel at the highest magnification (~210×) for a field of view of 0.94 × 0.70 mm^2, similar to previous studies (Koutsiaris et al., 2007; Shahidi et al., 2010). The setting provides ~5 pixels for one RBC. The system can be set to 4.38 μm per pixel at the low magnification (~70×) for a field of view of 2.82 × 2.10 mm^2, similar to the CAIM setting (Cheung et al., 2001b). This setting provides about 1.5 pixels for one RBC. To capture the movement of RBC aggregates, a suitable temporal resolution achieved by a high recording speed is needed. As a rule of thumb, reliable estimations can be obtained for speeds of up to a 10-pixel shift per image (Deneux et al., 2012). Our system has 60 fps which is enough to capture RBC velocities of up to 2.6 mm/s. These similar approaches have been proven to successfully capture blood flow velocities in previous studies (Koutsiaris et al., 2010; Shahidi et al., 2010). A green filter was used because the light absorption by RBCs is much stronger than the one from the surrounding plasma and tissues (Bollinger et al., 1974; Butti et al., 1975; Deneux et al., 2012).

Vessels on the temporal bulbar conjunctiva were recorded at multiple locations using the highest magnification setting. Custom software was developed to process the video clips, based on space-time images on the bulbar conjunctiva (Shahidi et al., 2010). The software developed in Matlab (Ver. R2012a, 32-bit, Mathworks, Inc., Natick, MA) with all toolboxes included in the Total Academic Headcount Campus license, displayed the first image of a video clip acquired on the bulbar conjunctiva (Fig. 3A). Area based image registration technique was applied to compensate eye motion. The first image in the video clip was the reference frame. A manually selected box (blue box in Fig. 3B) containing vessel intersections in the first image was used as the reference frame window. Search windows were from the subsequent images. Normalized cross-correlation of the reference frame window and search windows in the non-registered frames was calculated. The largest correlation coefficients determined the translation/registration of each subsequent image to the reference frame. After each frame of the video clip was co-registered to compensate for eye movements, each frame was averaged and the averaged image was processed to segment all vessels and marked the center lines of the vessels in red (Fig. 3C). Vessel

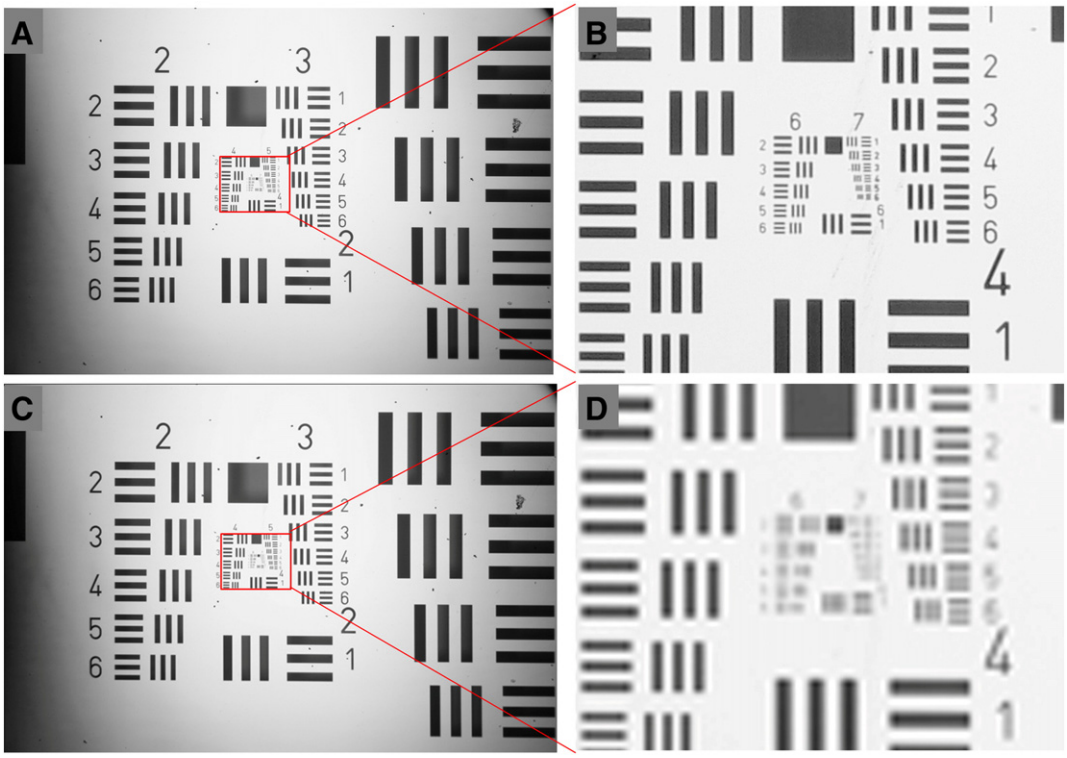

Fig. 1. Illustration of Movie Crop Function. The US Air Force 1951 resolution test card (A) was imaged with the maximum resolution of 5184 × 3456 pixels (17.9 megapixels) with the field of view of 7.61 × 5.04 mm^2 (1.47 μm per pixel). Cropped image from the center portion of 640 × 480 pixels (B) simulated the image used in the Movie Crop Function for high speed video recording with 7.5× magnification for telephoto effect. The black and white bars are readable at the element 3 of the group 7 of the resolution card. To compare with the digital zoom approach, the image was resized from Image A to 720 × 480 pixels, which is used to record standard definition video sequence without the Movie Crop Function. The image was then resized back to 5184 × 3456 pixels (C). Same center portion of 640 × 480 pixels from Image C was cropped (D). The smallest bars of Image D are readable at the element 4 of the group 5. Note. The resolution of Image D is much worse than Image B.

centerlines were extracted by processing the mean image of the registered images. Enhancement and segmentation of vessels were accomplished using a modification of a technique described by Macgillivray and Patton (2006). Global image threshold was used to generate a binary image. After that, a series of morphological operations were performed to thin the vessel to generate a centerline, similar to these described by Shahidi et al. (2010). These morphological steps included: (1) removing the small objects and filling of the holes, (2) erosion followed by dilation, (3) skeletonization, and (4) deletion of short lines. The vessels of interest were manually selected (Fig. 3D). The software searched the center line and created the intensity profiles which were perpendicular to the center line. The vessel diameter was defined as the full width at the half-maximum (FWHM) of the intensity profile (Fig. 3F). The vessel wall was marked in green and blue lines (Fig. 3F). Averaged diameter of the 75 pixels marked as the length in these three colors (Fig. 3G) of the vessel was calculated.

In order to create a space-time image (STI) to measure the blood flow velocity, the intensities within the outlined diameter of each frame (purple area in Fig. 3F) were computed to create a reflectivity profile representing the vessel path length on the Y-axis (distance along vessel as the vertical line) (Figs. 3H and I). The X-axis was the time in the video. The prominent bands of blood flow were clearly visible (Fig. 3G) as the RBC aggregates moved. Two points located in the middle of two ends of each longest continuous high-intensity band were identified manually to create a line. The slopes of the line marked in red lines were calculated using a linear equation of $Y = mX + b$ (where m determines the slope and b is the intercept) (Fig. 3I) as the measurements of axial blood flow velocity. Multiple processes of the STI were conducted to yield all results in these selected vessels. The graphical user interface (GUI) demonstrated the procedure and displayed the results which included vessel diameter, axial and cross-sectional blood flow velocity as well as blood flow rate (Fig. 4). The cross-sectional blood flow velocities and flow rates were calculated based on the equation previously published (Koutsiaris et al., 2007). Using this equation, the velocity profile across the vessel width were taken into account for estimating the cross-sectional velocity and volume flow by the authors (Koutsiaris et al., 2007), in contrast to others (Deneux et al., 2012) who considered the velocity profile to be flat.

Calibration of measuring bulbar conjunctival red blood cell velocity

The FSLB calibration of measuring axial blood velocity was based on the simulation described by Maryrovitz and Larnard (Mayrovitz et al., 1981). They used an infusion pump to move a calibration slide and a blood smear for calibrating velocities using video recording. The moving target was tracked frame by frame in the video sequence. The infusion pump moved at a known speed and velocity calculation was based on the distance the target moved within a given time. We put a drop of human blood sandwiched between two microscope slides. The slides were attached on an infusion pump (UMP2, World Precision Instruments, Sarasota, FL, USA), which moved at a known velocity (Fig. 5). The pump was set for velocities ranged from 0.05 mm/s to 1.73 mm/s. The moving blood film was recorded at each setting and video clips were processed using the same custom software mentioned above used for processing bulbar conjunctival blood flow velocity. The measured velocities were nearly identical to the known velocities set with the pump (Fig. 6).

Imaging bulbar conjunctival nMPMs and fractal analysis

We developed a single shot method to generate the nMPMs with only one image by FSLB. With a built-in green filter and a 22× magnification, the field of view was about 15.74 × 10.50 mm^2. A diffuse filter was used to take the 5184 × 3456 pixel image of the temporal bulbar

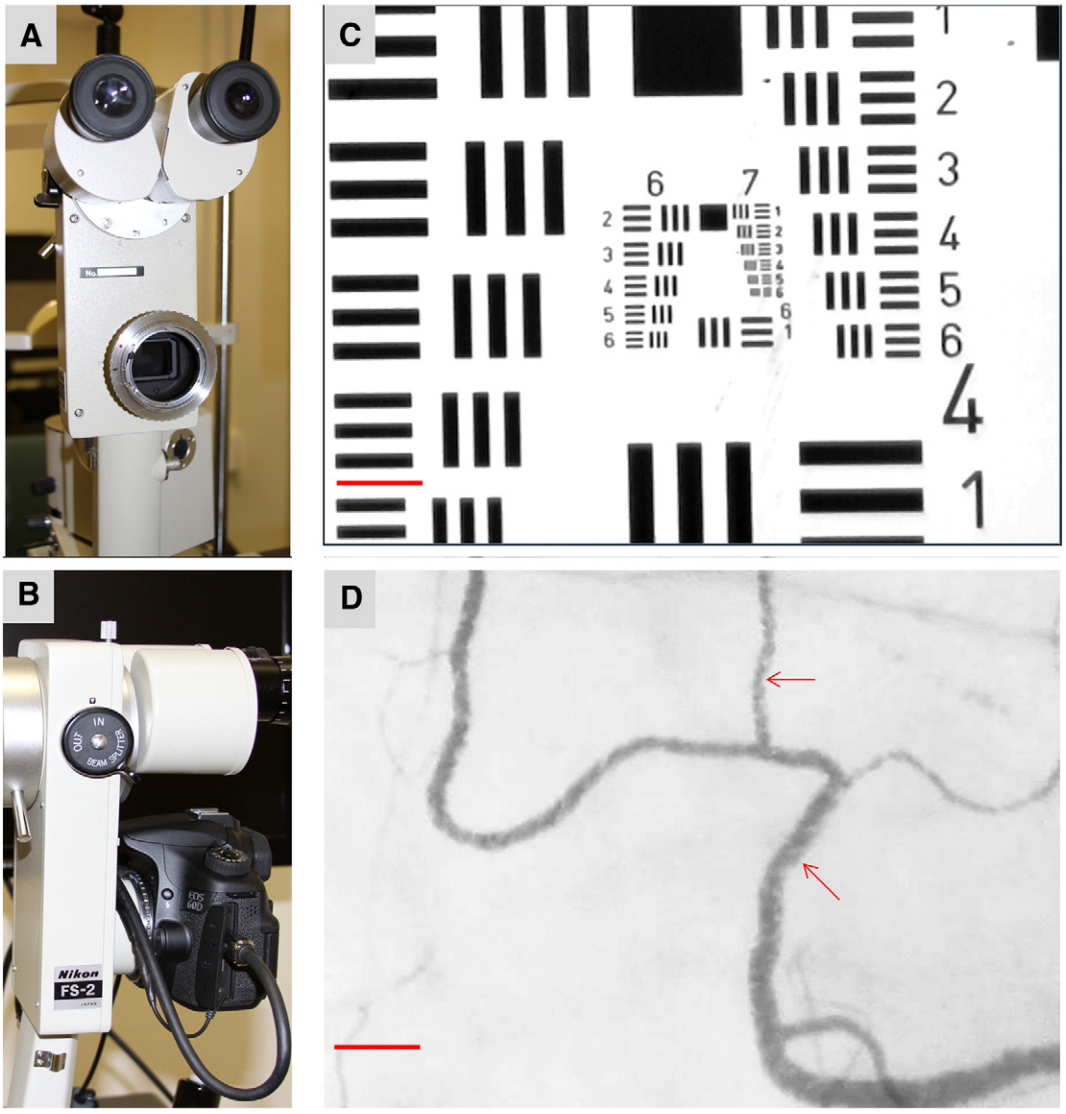

Fig. 2. Functional slit-lamp biomicroscopy (FSLB). A traditional slit-lamp (Nikon FS-2, Nikon Inc., Melville, NY) (A) was used and a digital camera (Canon 60D, Canon Inc., Melville, NY) was attached via an inherent camera port (B). The spatial display resolution was tested using a resolution test card (US Air Force 1951, Edmund Optics Inc., Barrington, NJ) (C) and the element 3 of group 7 was readable, corresponding to the resolution of 161 line pairs/mm. The width of the black or while line of the element 3 in group 7 is 3.11 μm. With the inherent optical magnification of 30× and additional 7.5× magnification provided by the Movie Crop Function, the total magnification was ~210×, which is sufficient to image the movement of red blood cell aggregates. A captured still image (D) from a video sequence was obtained on the temporal bulbar conjunctiva of a normal subject with FSLB. Clusters of red blood cells (red arrows) are clearly visible. Red bars = 100 μm.

conjunctiva (Fig. 7A). Custom software was developed in Matlab (Mathworks, Inc., Natick, MA). The processing procedure was similar to these reported previously for segmenting the retinal non-invasive capillary perfusion maps (nCPMs) (Jiang et al., 2013a). Compared to the procedure for processing the retinal nCPMs, the raw image of the conjunctiva (Fig. 7A) did not need to invert, but the image was resized to 1024 × 683 pixels. After correcting non-uniform illumination using adaptive histogram equalization for the enhancement of the vessel and background (Fig. 7B), morphological opening operations, which consisted of erosion followed by dilation, were conducted to remove background noise and eliminate non-vessel structures. The procedure involved the supremum of the openings with a linear structuring element [se = strel ('line',10,0)] at 18 rotations each 10° apart to enhance the vessel along the vessel direction, and the infima of the openings as the background which was subtracted from the enhanced vessel image (Fig. 7C). The vessels were segmented using thresholding (Fig. 7D). The procedure mentioned above was fully automated using the custom software. Using ImageJ (NIH, Bethesda, MD), the image (Fig. 7D) was cropped into 512 × 512 pixels which covered 7.87 × 7.87 mm^2 near the limbus (Fig. 7E), which was then inverted (Fig. 7F). After making binary of the image, the image was skeletonized (Fig. 7G) and then inverted (Fig. 7H) which was ready for fractal analysis (Figs. 7I and J). Raw images before (Fig. 8A) and after contact lens wear (Fig. 8D) were used to process the nMPMs (Figs. 8B and E) and create skeletonized images (Figs. 8C and F).

We used the fractal analysis toolbox from Benoit™ (TruSoft Benoit Pro 2.0, TruSoft Inc., St. Petersburg, FL) to analyze the fractal dimension of the segmented bulbar conjunctival nMPMs. Benoit™ is a piece of commercial software enabling fractal analysis for measuring the fractal dimension in Windows environment. The software has a toolbox version for Mathlab, called Benoit for Matlab. We used the software in Windows 7 to conduct our study. We processed the segmented nMPMs using both monofractal (Dbox) and multifractal (D0) analyses (Figs. 7I and J).

Human study

A human study including six human subjects was conducted. This protocol was approved by the institutional review board for human

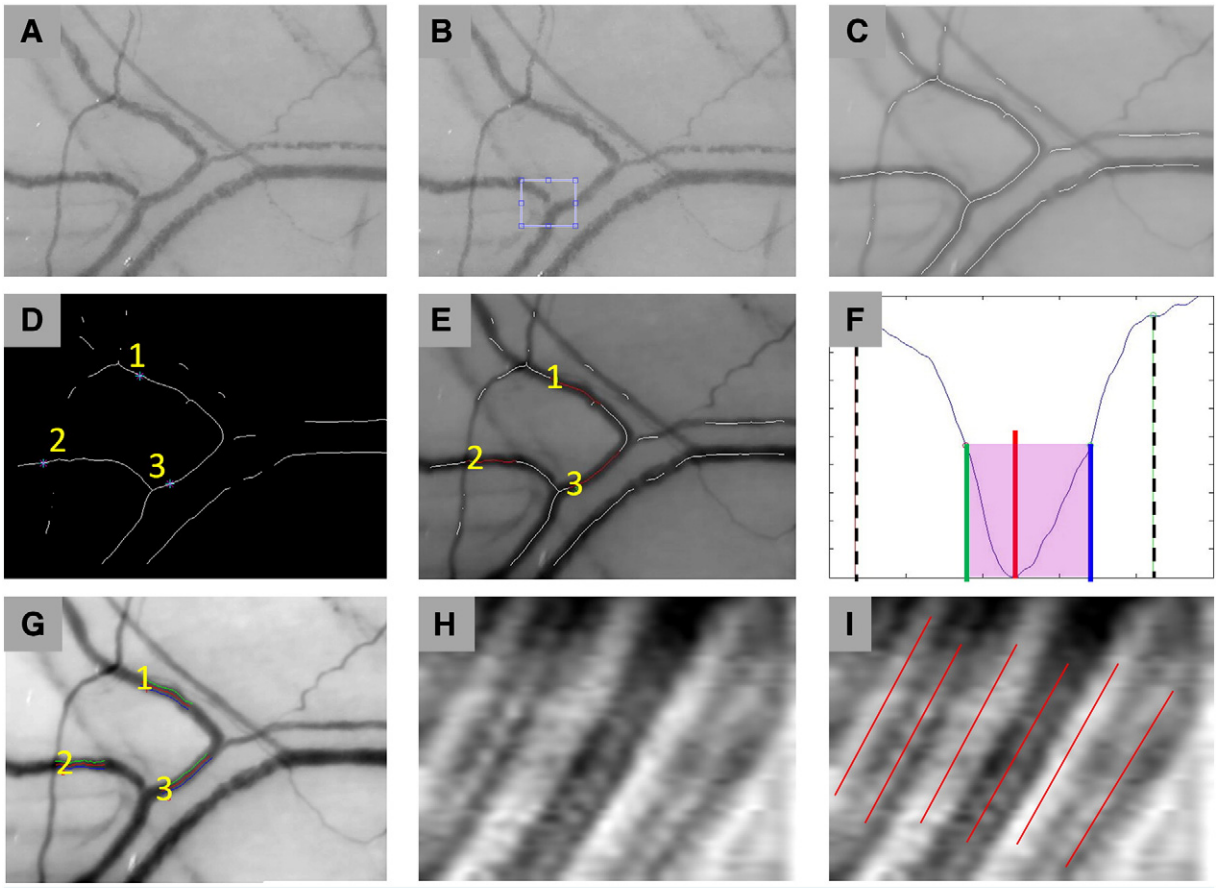

	Mean Diameter (μm)	Axial Velocity (mm/s)	Cross-sectional Velocity (mm/s)	Flow Rate (pl/s)
1	28.48	0.47	0.32	202.88
2	26.72	0.08	0.05	30.08
3	27.10	0.49	0.33	193.15

Fig. 3. Image processing to measure vessel diameter and blood flow velocity. Custom software was developed to process the video clip obtained on the bulbar conjunctiva. The first image (A) of a video clip was displayed and manually selected box (blue box in Image B) containing a triangle of the blood vessels was used for registration of all frames of the video for compensating eye movements. Vessels were segmented from averaged image of all frames in the video and center lines of the vessels were marked in red (C). The vessels of interest were manually selected as marked in the asterisk and numbers (D). The software searched the center line of 75 pixels (E) and created the intensity profiles which were perpendicular to the center line (F). The vessel diameter was defined as the full width at the half-maximum (FWHM) of the intensity profile (F). The vessel wall was marked in green and blue lines (F). A space-time image (STI) was used to measure the blood flow velocity. The intensities within the outlined diameter of each frame (the purple area) were computed to create a reflectivity profile representing the vessel path length on the Y-axis (distance along vessel) and used as the vertical line of a time point (H and I). The X-axis was the time in the video and each time point represented each frame in the video sequence. The prominent bands of blood flow were clearly visible (G) as the RBC aggregates moved. The slopes of the bands were manually outlined and marked in red lines (H) and calculated as the measurements of axial blood flow velocity. Further calculations yielded the cross-sectional blood flow velocities and flow rates, as listed below.

research at the University of Miami, informed consent was obtained from each subject, and all subjects were treated in accordance with the tenets of the Declaration of Helsinki. In this prospective study, there were 6 human subjects (2 males and 4 females) enrolled. Their mean age was 37.7 ± 17.7 years (range 25 to 49 years). Exclusion criteria were anterior or posterior segment pathology of eye; history of laser treatment, trauma, or eye surgery; systemic disease; tobacco or alcohol use; or on any medication. Excluded compounding factors included hypertension, diabetes, sickle cell anemia, cerebral small vessel disease, stroke and other cardiovascular/cerebrovascular diseases or other vascular diseases.

After 10 min of rest, the subject moved into position by placing the chin on the chin rest of the FSLB. The subject fixed at a specific target at an angle of approximately 40° to the nasal side. The green filter was used in the path of the slit-lamp illumination light. The operator adjusted the distance between the slit-lamp microscopy and the temporal bulbar conjunctiva of the subject's eye for sharply focusing on the bulbar conjunctival vessels by observing the live view image on the HD monitor. At 22× magnification of the slit-lamp, still images of the temporal bulbar conjunctiva were taken to obtain the microvascular network. At the 210× magnification, video clips were recorded for measuring the bulbar conjunctival microvascular circulation. Multiple locations were recorded and each location included several vessels. At least 5 venules were recorded. Each microvessel was recorded for 1 to 2 s and the total time of the procedure was about 3 to 5 min. Because the bulbar conjunctival microvascular network has unique shape, each vessel of interest can be easily re-located for a longitudinal study. The same vessels were recorded at baseline before wearing the lens and 6 h after wearing the lens with the lens on.

Results

The blood flow was successfully captured and analyzed in all images obtained from the human subject. In the video clips, the movement of the cluster of blood red cells was clearly noticeable. At baseline, the venular blood flow rate was found to relate to the vessel diameters

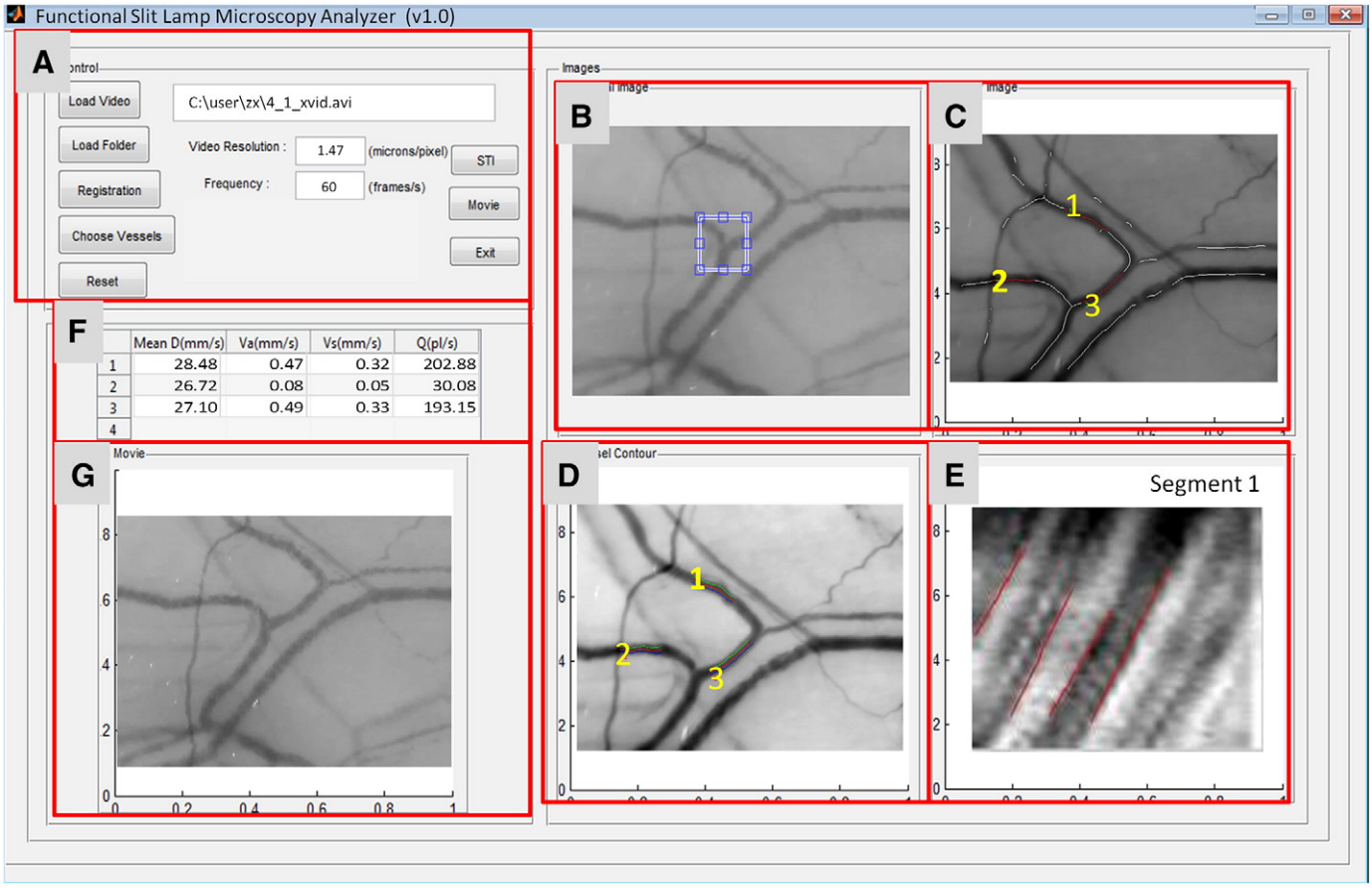

Fig. 4. Graphical user interface (GUI) of functional slit lamp biomicroscopy analyzer. A, video input and setting. B, manual selection of a small window for registration of video sequences; C, selection of vessels of interest on the segmented vessels; D, displaying the segmented results of vessel width; E, manual outline of a space time image (STI); F, results; G, playing registered video.

(Fig. 9), however, the relations between the venular vessel width and blood flow velocities were not evident. The mean bulbar conjunctival venular vessel diameter was 18.8 ± 2.7 μm (range 9.4–28.0 μm) at baseline and increased to 19.6 ± 2.4 μm (range 9.6–28.2 μm) after 6 h of lens wear (paired *t*-test, P = 0.020). The venular axial blood flow velocity was increased from 0.60 ± 0.12 mm/s (range 0.11–1.18 mm/s) to 0.88 ± 0.21 mm/s (range 0.23–1.48 mm/s)(P = 0.001). The venular cross sectional blood flow velocity was increased from 0.43 ± 0.08 mm/s (range 0.08–0.83 mm/s) to 0.62 ± 0.15 mm/s (range 0.16–1.02 mm/s)(P = 0.001). The venular blood flow rate was also increased

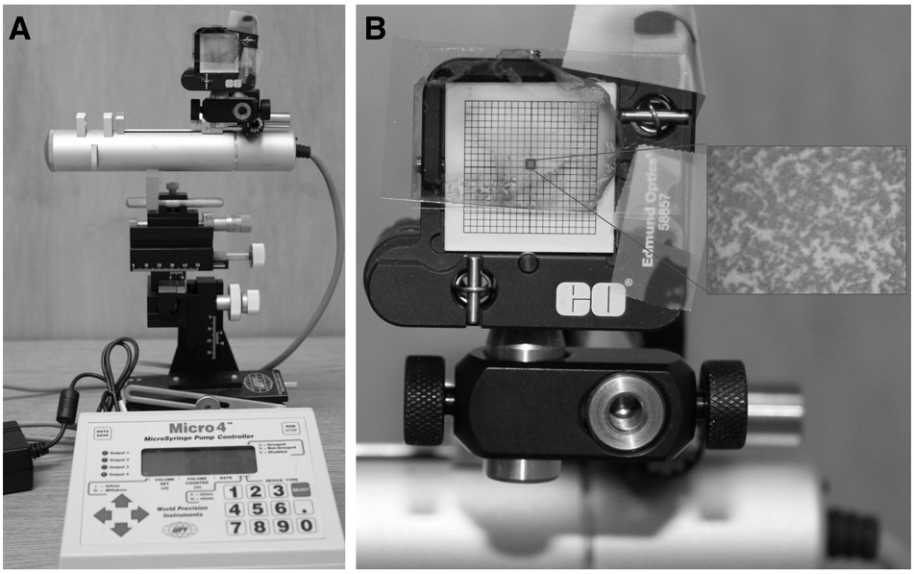

Fig. 5. Calibration of measuring bulbar conjunctival red blood cell velocity. A microscope slide with a drop of human blood covered with a cover slide was mounted on an infusion pump using tapes (A). In the background, a line grid target (Edmund Optics Inc., Barrington, NJ) was mounted on a Edmund kinematic mount which facilitated the focusing and the adjustment of the blood film (B). The blood film was imaged using the slit-lamp in the center of the blood film as shown in the insert of image B.

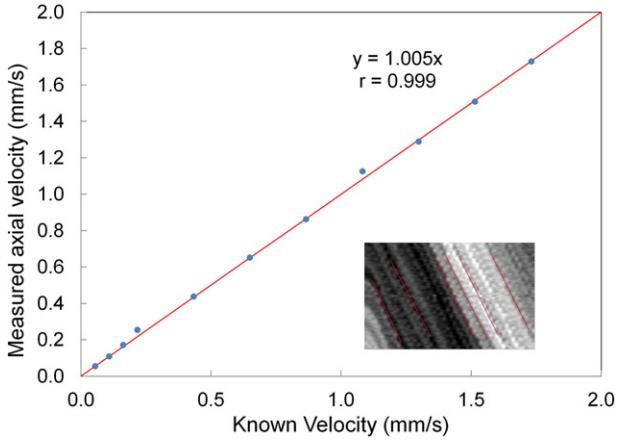

Fig. 6. Calibration of the measurement of blood flow velocity. A thin blood film sandwiched between two microscope slides mounted on an infusion pump was imaged with FSLB. The measured velocities were nearly identical to the velocity settings by creating the space-time image (insert). The solid line corresponds to the equality.

from 129.8 ± 59.9 pl/s (range 17.4–421.1 pl/s) to 207.2 ± 81.3 pl/s (range 25.0–521.8 pl/s) (P = 0.001) (Fig. 10).

Bulbar conjunctival nMPMs showed the intricated details of the microvascular network. At baseline, fractal dimension was 1.63 ± 0.05 and 1.71 ± 0.03 analyzed by monofractal and multifractal analyses, respectively. Significant increases in fractal dimensions obtained with both monofractal (1.69 ± 0.03) and multifractal analyses (1.76 ± 0.03) were found after 6 h of lens wear (P = 0.02) (Fig. 10).

Discussion

Developing and validating clinical friendly bulbar conjunctival microvascular imaging may lead to more accessible ways to study systemic and cerebral vasculopathies in addition to ocular diseases. In the present study, microvascular network morphology and hemodynamics (blood flow velocity and rate) were measured with FSLB, which enabled investigating the relationship between them. Our approach has some advantages compared to the previous instruments. Several methods have been developed for measuring the bulbar conjunctival blood flow (Duench et al., 2007; Jiang et al., 2013b; Koutsiaris et al., 2010). Methods and measurements of blood velocity are different in venules than in arterioles. Shahidi et al. (2010) and Koutsiaris et al. (2007) measured the blood flow velocity in human conjunctival venules. Koutsiaris et al. (2010, 2013) measured it in human conjunctival arterioles.

We previously adapted the Retinal Function Imager (RFI, Optical Imaging Ltd., Rehovot, Israel) for imaging the bulbar conjunctival microvasculature, creating bulbar conjunctival nMPMs and measuring blood flow velocity (Jiang et al., 2013b). Due to the difficulty of building complicated optics into the imaging modality for imaging the blood red cell movement in previously reported instruments as well as the high cost of some of these devices (e.g. the RFI), functional imaging of bulbar

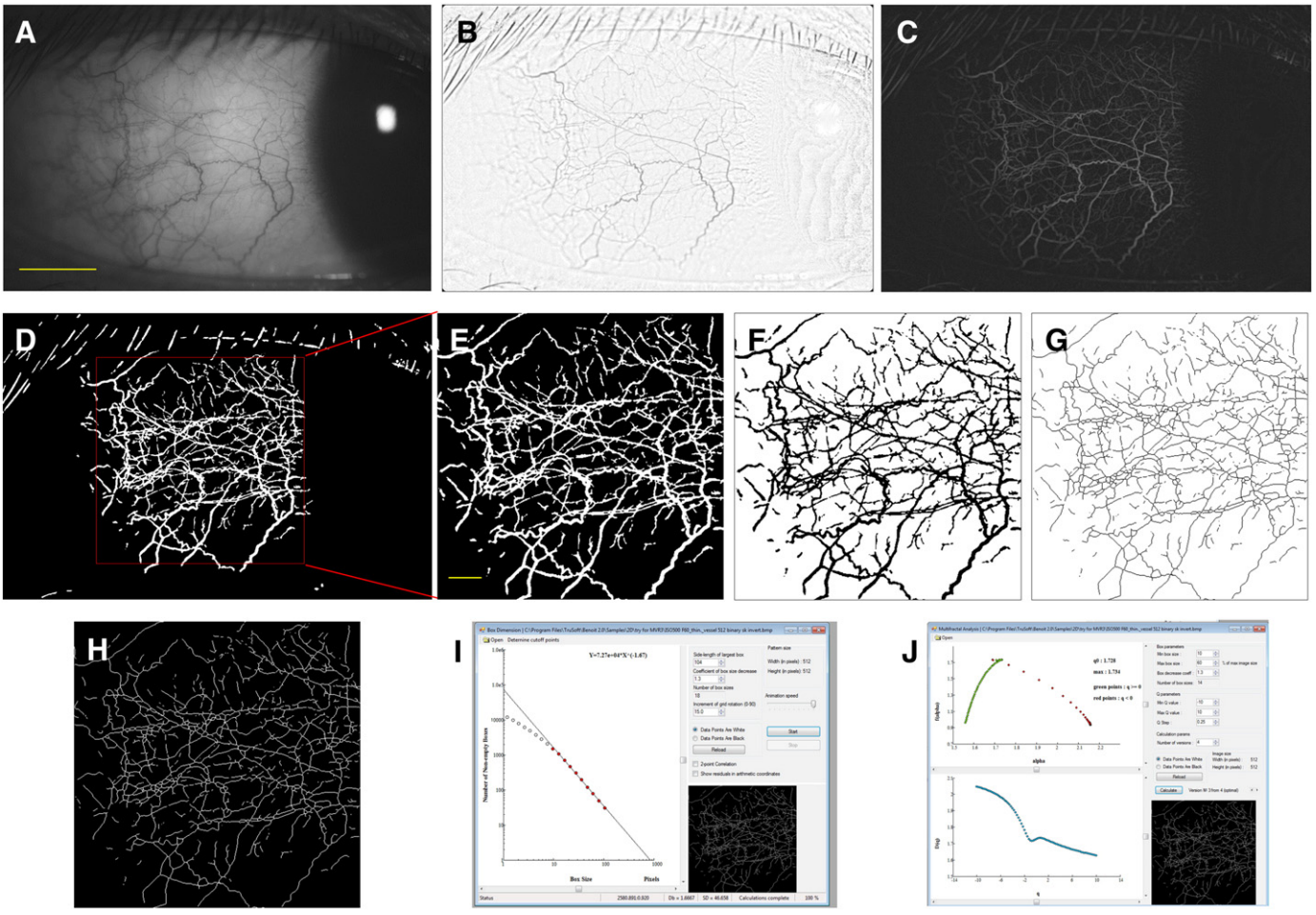

Fig. 7. Image processing of non-invasive microvascular perfusion maps (nMPMs) and fractal analysis. Custom software was developed to segment conjunctival vessels to create the nMPMs for fractal analysis. The raw image was resized from 5184 × 3456 pixels to 1024 × 683 pixels (A). B. Non-uniform illumination using adaptive histogram equalization. C. non-invasive microvascular perfusion map (nMPM) after morphological opening operations. D. Segmented vessels. E. Cropped image of 512 × 512 pixel with a field of view 7.87 × 7.87 mm^2. F. Inverted image. G. Skeletonized image. H. Inverted skeletonized image. I. Monofractal analysis using the box-counting to get the measurement of Dbox. J. Multifractal analysis to obtain the measurement of D0. Bars = 3 mm.

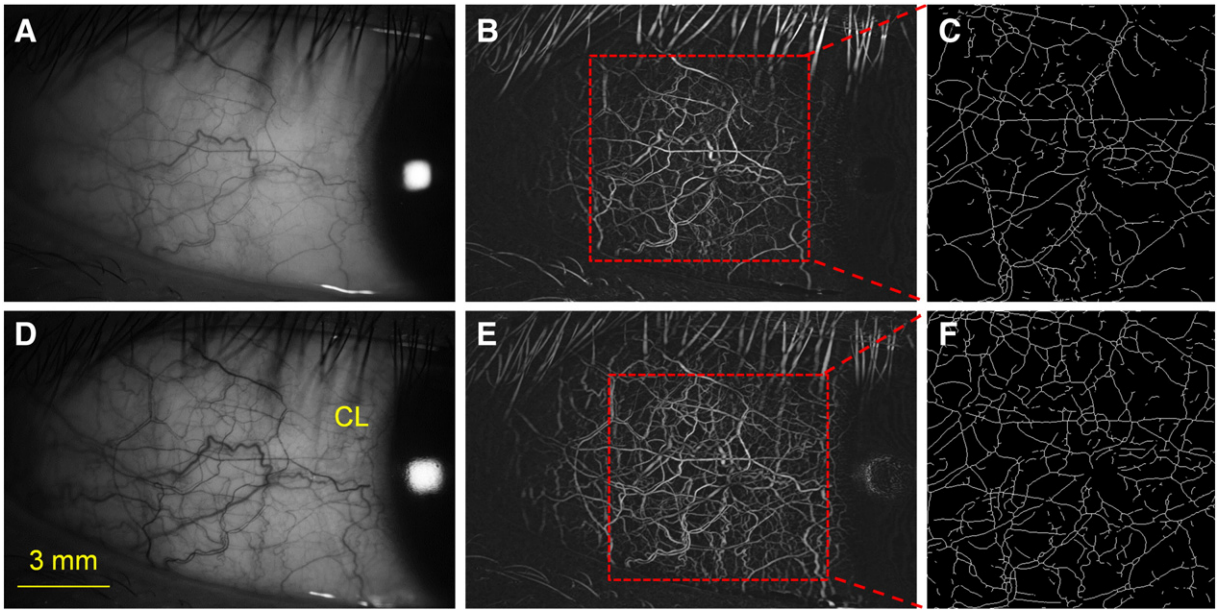

Fig. 8. Bulbar conjunctival microvascular network before and after wearing contact lenses. The temporal bulbar conjunctiva of a participant was imaged before (A–C) and after 6 h of lens wear (D–F) (magnification = 22×). The microvascular network of the bulbar conjunctiva was clearly visualized in the raw image (A and D), segmented vessel network (B and E) and skeletonized vessel network (C and F). After 6 h of lens wear, more vessels were visualized in the raw image, segmented vessel image and skeletonized image. CL = contact lens. The cropped area was 7.87 × 7.87 mm^2 in the temporal bulbar conjunctiva 1 mm away from the limbus.

conjunctival microvasculature has not been widely used in clinical research. Using a series of flashing lights, the bulbar conjunctival nMPMs acquired with the RFI device appeared not to show the intricated details of the capillaries, possibly due to saturation of the image on the sclera and low pixel resolution (Jiang et al., 2013b). Furthermore, information on vessel diameters could not be obtained due to the limited magnification and image size.

Compared to the RFI's derived nCPMs, FSLB derived nMPMs revealed greater details of the complex microvascular network, which was suitable for fractal analysis. The most advantageous feature of our approach is that the method can be used to image a wider field of the microvascular network and the details of the microvascular circulation. In addition, the use of a commercially available advanced high speed camera for adaptation into traditional slit-lamp biomicroscopy may enable the method to be used widely in patient care and research. The FSLB has taken the traditional slit-lamp microscopy to the next level by this novel approach that facilitated both an extremely high magnification and speed for imaging the bulbar conjunctival microcirculation. Because a complicated and expensive adaption is not needed, the FSLB is cost-effective. FSLB can be used to image both nMPMs and microcirculation's hemodynamics. In this study, the mean bulbar conjunctival blood flow velocity was approximately 0.6 mm/s, which is within the range reported by previous studies using other techniques by Koutsiaris et al. (approximately 0.20–1.70 mm/s) (Koutsiaris et al., 2007) and Shahidi et al. (0.20–1.20 mm/s) (Shahidi et al., 2010). Interestingly, we established the relationship between the vessel diameter and blood flow rate as a power law function, which was in agreement with previous findings by Shahidi et al. (2010) and Koutsiaris et al. (2007). The volume flow power law equation (Fig. 9) is very close to the one reported by Koutsiaris et al. (2007), which further validates the work. The quantitative analysis of the bulbar conjunctival microcirculation provides an easy way to study systemic small vessel diseases, including conditions affecting organs such as the heart, kidney and brain, over time in vivo.

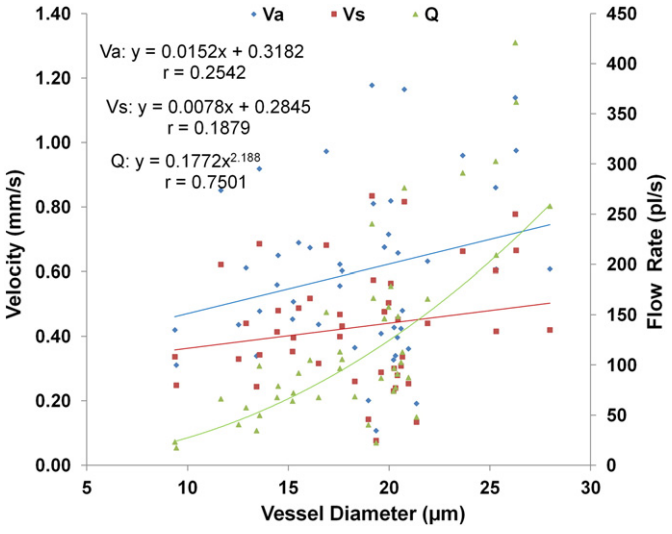

Fig. 9. Relations among vessel diameter and venular blood flow velocity and flow rate. A strong relation was evident between the vessel diameter and venular blood flow rate. Va = axial blood flow velocity; Vs = cross-sectional velocity; Q = blood flow rate.

The microvascular network on the bulbar conjunctiva appears to be very dense with a high level of complexity. There is orderly anastomosing of networks of capillaries, arterioles and venules around the avascular cornea. The ratio of the arterioles to venules is typically ~1:2, which exhibits an even distribution without the presence of dilations, narrowing, distension, microaneurysm and tortuosity (Fig. 1). The unique shapes and forms of the bulbar conjunctival microvasculature make it an ideal site for noninvasive real-time imaging of pathologic conditions and evaluations of therapies.

The characteristics of the vascular network can be evaluated using fractal analysis, which is a tool that is commonly used to analyze vascular branching networks in fundus images (Talu, 2011). Vasculopathies represented by fractal dimensional changes have been identified in stroke (Doubal et al., 2010), diabetic retinopathy (Cheung et al., 2009b) and ocular conditions (Schulze et al., 2008). Schulze et al. used fractal analysis to observe bulbar conjunctival redness/hyperemia and graded images using different scales for bulbar conjunctival redness (Schulze et al., 2008). The researchers' fractal analysis was based on images obtained using white illumination, which resulted in low image contrast for segmenting the vascular network.

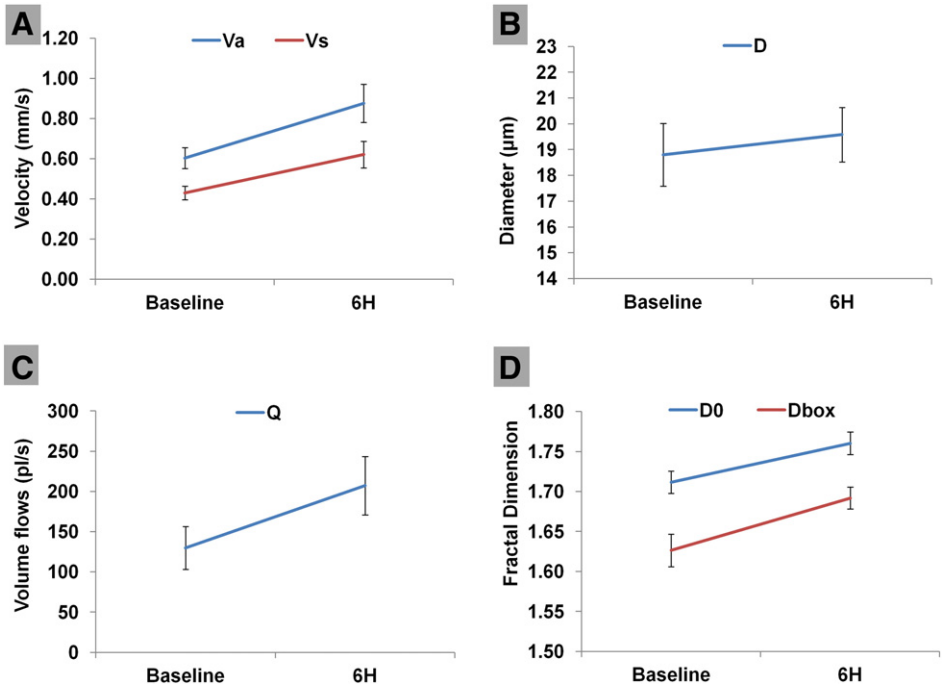

Fig. 10. Microvascular measurements before and after 6 h of wearing contact lenses. The axial blood flow velocity (Va), cross-sectional blood flow velocity (Vs), vessel diameter (D), blood flow rate (Q), mono- (Dbox) and multifractal (D0) dimensions were increased significantly after 6 h of lens wear compared to baseline (*t*-test, $P < 0.05$). Bars = Standard Error.

We obtained bulbar conjunctival microvascular images with green illumination. The contrast of the vessels appeared enhanced, which facilitated the automatic segmentation and fractal analysis. Compared to monofractal analysis, multifractal analysis has been confirmed to be more sensitive to subtle retinal changes in the vasculature because the retina appears to have multifractal properties (Doubal et al., 2010; Talu, 2013). As expected, the multifractal dimension was higher than the monofractal dimension in the bulbar conjunctiva, which is similar to what was observed in the retina (Doubal et al., 2010; Talu, 2013).

Fractal analysis was used to analyze the bulbar conjunctival microvascular network at the capillary level using the FSLB image. Automated segmentation was feasible to process the bulbar conjunctival nMPMs. The method could be easily and widely used in research and clinics. Microvascular networks have been roughly evaluated using the grading scales of bulbar conjunctival redness and limbal vascularization (Dumbleton et al., 2001; Efron, 1997; Schulze et al., 2008). For example, grading scales of bulbar conjunctival redness have been used to evaluate microvascular responses to contact lens wearing (Dumbleton et al., 2001; Efron, 1997; Schulze et al., 2008). Schulze et al. assessed bulbar conjunctival redness/hyperemia and found a strong correlation between photometric chromaticity measurements of bulbar conjunctival redness with hyperemia (Schulze et al., 2008). However, the redness scales and estimation of limbal vascularization may not be sensitive enough for a quantitative evaluation of the microvascular morphologic network. Our method has been validated in measuring the ocular microvascular response to contact lens wear. Evidence indicates that wearing CLs causes bulbar conjunctival microvascular changes, such as vessel compression or occlusion, blood flow intermission, and increased vascular tortuosity (Cheung et al., 2012). CL-related acute red eye (CLARE) as a circumlimbal hyperemia is a good example of the vascular response to CL wear (Holden et al., 1986). In clinical trials, the grading of bulbar conjunctival redness has been used as a surrogate marker of bulbar conjunctival vascular response and has been regarded as one of the endpoints of CL fitting and tolerance. Our study demonstrated the microvascular responses can be quantitatively evaluated by measuring the network and circulation using FSLB.

As expected, the increases in all measured parameters in a small sample size may indicate the sensitivity of the method in determining the vascular responses. This may open a new era for evaluating contact lens fitting and its interaction with ocular surface. This may also help to better understand impacting factors to ocular discomfort during contact lens, a common and serious issue in contact lens wearers.

In conclusion, we demonstrate FSLB for quantitatively measurement of fractality of bulbar conjunctival microvascular network, morphometry and hemodynamics. The alternations of the fractal dimensions, morphometry and hemodynamics during contact lens wear may indicate ocular microvascular responses to contact lens wear. Future work will focus on the further characterization of human bulbar conjunctival microvasculature in ocular, systemic and central nervous system diseases.

Acknowledgments

Grant/financial support: Supported in part by the research grants NIH R01EY020607, and R01EY020607S, NIH Center Grant P30 EY014801 and a grant from the Research to Prevent Blindness (RPB).

Commercial relationship: None.

Financial Disclosures: The University of Miami and Drs Jiang, Cabrera DeBuc and Wang hold a pending patent of the technique used in the study and have the potential for financial benefit from its future commercialization. All other authors have no proprietary interest in any materials or methods.

References

Avakian, A., Kalina, R.E., Sage, E.H., Rambhia, A.H., Elliott, K.E., Chuang, E.L., Clark, J.I., Hwang, J.N., Parsons-Wingerter, P., 2002. Fractal analysis of region-based vascular change in the normal and non-proliferative diabetic retina. Curr. Eye Res. 24, 274–280.

Azemin, M.Z., Kumar, D.K., Wong, T.Y., Kawasaki, R., Mitchell, P., Wang, J.J., 2011. Robust methodology for fractal analysis of the retinal vasculature. IEEE Trans. Med. Imaging 30, 243–250.

Bollinger, A., Butti, P., Barras, J.P., Trachsler, H., Siegenthaler, W., 1974. Red blood cell velocity in nailfold capillaries of man measured by a television microscopy technique. Microvasc. Res. 7, 61–72.

Butti, P., Intaglietta, M., Reimann, H., Holliger, C., Bollinger, A., Anliker, M., 1975. Capillary red blood cell velocity measurements in human nailfold by videodensitometric method. Microvasc. Res. 10, 220–227.

Cheung, A.T., Perez, R.V., Chen, P.C., 1999. Improvements in diabetic microangiopathy after successful simultaneous pancreas-kidney transplantation: a computer-assisted

intravital microscopy study on the conjunctival microcirculation. Transplantation 68, 927–932.
Cheung, A.T., Harmatz, P., Wun, T., Chen, P.C., Larkin, E.C., Adams, R.J., Vichinsky, E.P., 2001a. Correlation of abnormal intracranial vessel velocity, measured by transcranial Doppler ultrasonography, with abnormal conjunctival vessel velocity, measured by computer-assisted intravital microscopy, in sickle cell disease. Blood 97, 3401–3404.
Cheung, A.T., Ramanujam, S., Greer, D.A., Kumagai, L.F., Aoki, T.T., 2001b. Microvascular abnormalities in the bulbar conjunctiva of patients with type 2 diabetes mellitus. Endocr. Pract. 7, 358–363.
Cheung, A.T., Tomic, M.M., Chen, P.C., Miguelino, E., Li, C.S., Devaraj, S., 2009a. Correlation of microvascular abnormalities and endothelial dysfunction in Type-1 Diabetes Mellitus (T1DM): a real-time intravital microscopy study. Clin. Hemorheol. Microcirc. 42, 285–295.
Cheung, N., Donaghue, K.C., Liew, G., Rogers, S.L., Wang, J.J., Lim, S.W., Jenkins, A.J., Hsu, W., Li, L.M., Wong, T.Y., 2009b. Quantitative assessment of early diabetic retinopathy using fractal analysis. Diabetes Care 32, 106–110.
Cheung, N., Liew, G., Lindley, R.I., Liu, E.Y., Wang, J.J., Hand, P., Baker, M., Mitchell, P., Wong, T.Y., 2010. Retinal fractals and acute lacunar stroke. Ann. Neurol. 68, 107–111.
Cheung, A.T., Hu, B.S., Wong, S.A., Chow, J., Chan, M.S., To, W.J., Li, J., Ramanujam, S., Chen, P.C., 2012. Microvascular abnormalities in the bulbar conjunctiva of contact lens users. Clin. Hemorheol. Microcirc. 51, 77–86.
Deneux, T., Takerkart, S., Grinvald, A., Masson, G.S., Vanzetta, I., 2012. A processing workflow for measuring erythrocytes velocity in extended vascular networks from wide field high-resolution optical imaging data. Neuroimage 59, 2569–2588.
Doubal, F.N., Macgillivray, T.J., Patton, N., Dhillon, B., Dennis, M.S., Wardlaw, J.M., 2010. Fractal analysis of retinal vessels suggests that a distinct vasculopathy causes lacunar stroke. Neurology 74, 1102–1107.
Duench, S., Simpson, T., Jones, L.W., Flanagan, J.G., Fonn, D., 2007. Assessment of variation in bulbar conjunctival redness, temperature, and blood flow. Optom. Vis. Sci. 84, 511–516.
Dumbleton, K.A., Chalmers, R.L., Richter, D.B., Fonn, D., 2001. Vascular response to extended wear of hydrogel lenses with high and low oxygen permeability. Optom. Vis. Sci. 78, 147–151.
Efron, N., 1997. Contact lens-induced conjunctival hyperaemia. Optician 213, 22–27.
Holden, B.A., Sweeney, D.F., Swarbrick, H.A., Vannas, A., Nilsson, K.T., Efron, N., 1986. The vascular response to long-term extended contact lens wear. Clin. Exp. Optom. 69, 112–119.
Jiang, H., Debuc, D.C., Rundek, T., Lam, B.L., Wright, C.B., Shen, M., Tao, A., Wang, J., 2013a. Automated segmentation and fractal analysis of high-resolution non-invasive capillary perfusion maps of the human retina. Microvasc. Res. 89, 172–175.
Jiang, H., Ye, Y., Debuc, D.C., Lam, B.L., Rundek, T., Tao, A., Shao, Y., Wang, J., 2013b. Human conjunctival microvasculature assessed with a retinal function imager (RFI). Microvasc. Res. 85, 134–137.
Koutsiaris, A.G., Tachmitzi, S.V., Batis, N., Kotoula, M.G., Karabatsas, C.H., Tsironi, E., Chatzoulis, D.Z., 2007. Volume flow and wall shear stress quantification in the human conjunctival capillaries and post-capillary venules in vivo. Biorheology 44, 375–386.
Koutsiaris, A.G., Tachmitzi, S.V., Papavasileiou, P., Batis, N., Kotoula, M.G., Giannoukas, A.D., Tsironi, E., 2010. Blood velocity pulse quantification in the human conjunctival precapillary arterioles. Microvasc. Res. 80, 202–208.
Koutsiaris, A.G., Tachmitzi, S.V., Batis, N., 2013. Wall shear stress quantification in the human conjunctival pre-capillary arterioles in vivo. Microvasc. Res. 85, 34–39.
Liew, G., Wang, J.J., Cheung, N., Zhang, Y.P., Hsu, W., Lee, M.L., Mitchell, P., Tikellis, G., Taylor, B., Wong, T.Y., 2008. The retinal vasculature as a fractal: methodology, reliability, and relationship to blood pressure. Ophthalmology 115, 1951–1956.
Lim, S.W., Cheung, N., Wang, J.J., Donaghue, K.C., Liew, G., Islam, F.M., Jenkins, A.J., Wong, T.Y., 2009. Retinal vascular fractal dimension and risk of early diabetic retinopathy: a prospective study of children and adolescents with type 1 diabetes. Diabetes Care 32, 2081–2083.
Macgillivray, T.J., Patton, N., 2006. A reliability study of fractal analysis of the skeletonised vascular network using the "box-counting" technique. Conf. Proc. IEEE Eng. Med. Biol. Soc. 1, 4445–4448.
Mayrovitz, H.N., Larnard, D., Duda, G., 1981. Blood velocity measurement in human conjunctival vessels. Cardiovasc. Dis. 8, 509–526.
Ohtani, N., 1996. Laser Doppler flowmetry of the bulbar conjunctiva as a monitor of the cerebral blood flow. Nihon Kyobu Geka Gakkai Zasshi 44, 1721–1728.
Schaser, K.D., Settmacher, U., Puhl, G., Zhang, L., Mittlmeier, T., Stover, J.F., Vollmar, B., Menger, M.D., Neuhaus, P., Haas, N.P., 2003. Noninvasive analysis of conjunctival microcirculation during carotid artery surgery reveals microvascular evidence of collateral compensation and stenosis-dependent adaptation. J. Vasc. Surg. 37, 789–797.
Schreiber, S., Bueche, C.Z., Garz, C., Braun, H., 2013. Blood brain barrier breakdown as the starting point of cerebral small vessel disease? — new insights from a rat model. Exp. Transl. Stroke Med. 5, 4.
Schulze, M.M., Hutchings, N., Simpson, T.L., 2008. The use of fractal analysis and photometry to estimate the accuracy of bulbar redness grading scales. Invest. Ophthalmol. Vis. Sci. 49, 1398–1406.
Shahidi, M., Wanek, J., Gaynes, B., Wu, T., 2010. Quantitative assessment of conjunctival microvascular circulation of the human eye. Microvasc. Res. 79, 109–113.
Talu, S., 2011. Fractal analysis of normal retinal vascular network. Oftalmologia 55, 11–16.
Talu, S., 2013. Multifractal geometry in analysis and processing of digital retinal photographs for early diagnosis of human diabetic macular edema. Curr. Eye Res. 38, 781–792.
To, W.J., Telander, D.G., Lloyd, M.E., Chen, P.C., Cheung, A.T., 2011. Correlation of conjunctival microangiopathy with retinopathy in type-2 diabetes mellitus (T2DM) patients. Clin. Hemorheol. Microcirc. 47, 131–141.
Ye, Y., Jiang, H., Zhang, H., Karp, C.L., Zhong, J., Tao, A., Shao, Y., Wang, J., 2013. Resolution of slit-lamp microscopy photography using various cameras. Eye Contact Lens 39, 205–213.